ICAS 2020 SHANG HAI
International Council of the Aeronautical Sciences
32nd Congress of the International Council of the Aeronautical Sciences
September 6-10, 2021
Pudong Shangri-La, Shanghai, China

LONGITUDINAL AND LATERAL-DIRECTIONAL AERODYNAMICS OF A RE-USABLE HIGH-SPEED VEHICLE

Tamás Bykerk[1], Giuseppe Pezzella[2], Dries Verstraete[3], and Antonio Viviani[2]

[1] Honorary Associate, the University of Sydney, Australia
[2] University of Campania, Engineering Department. Aversa (CE). Italy.
[3] University of Sydney, School of Aerospace, Mechanical and Mechatronic Engineering. Sydney. Australia.

Abstract

Re-usable, unmanned flying-test bed vehicles are an efficient way to experimentally validate next generation high-speed technologies. During the flight test phase, the aircraft will encounter free-stream velocities ranging from hypersonic to low subsonic, which requires a careful choice for the aeroshape. For the mission to be successful, the vehicle will need to be stable and maneuverable during both low and high-speed phases of flight. In this framework, the paper focused attention on both experimental and numerical flowfield investigations carried out on a spatuled-body vehicle aeroshape. Wind tunnel results from an early low speed test campaign, carried out by the University of Sidney, performed to validate subsonic computational fluid dynamics studies are provided and discussed. Results of Mach 7 flowfield simulations are analyzed to understand the high-speed behavior of the aircraft. Findings of this study pointed out that the vehicle requires a moment reference centre located at 45% of its length for static stability at both high and low speeds. Control deflection studies showed that the first estimate of elevon sizing is sufficient and the aircraft can easily be trimmed. Aeroshape Aerodynamics assessment is further on-going. Analyses are focusing on vehicle longitudinal and lateral-directional performance appraisal for different angles of attack and sideslip, elevons, ailerons and ruddervators deflections. Results are detailed reported and discussed in the paper.

Keywords: Subsonics; Hypersonics; CFD; Static Stability; Wind Tunnel Testing; Flying test bed.

1. Introduction

Technology advancements in next generation high-speed aircraft (HAS) strongly rely on the development of flying-test bed [1]. In fact, performing flight and Wind Tunnel (WT) test campaigns represents the only and ultimate proof to demonstrate the technical feasibility of new promising HAS concepts [2], [3]. In this framework, the paper reports on some results of the V-one project, jointly carried out by University of Sydney and University of Campania through both numerical and WT test activities, where the concept aeroshape, namely V-one, shown in Figure 1 is investigated [4],[5].

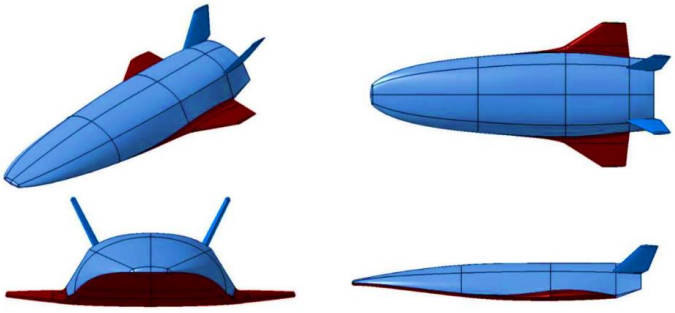

Figure 1 – Aeroshape concept four views [4], [5].

The V-one research programme aims to create the basis for a step-by-step increase of the readiness level of several enabling technologies suitable for High-Speed (HS) hypersonic flight, concerning aeroshape aerodynamics assessment. The test-bed glider aeroshape features a classical lifting-body aeroshape which embodies all the features of an operational HSA, such as a low aspect ratio double-delta wing, two full movable vertical stabilizers in butterfly configuration, a spatuled fuselage forebody,

characterized by a rounded off two-dimensional leading edge, mated on top of the wing. The wing flap, which must be actuated as elevon and aileron, is shown in purple in Figure 2 along with the complete moving fins (ruddervators) in green. The ruddervators pivot point is located at 50% of the root chord length.

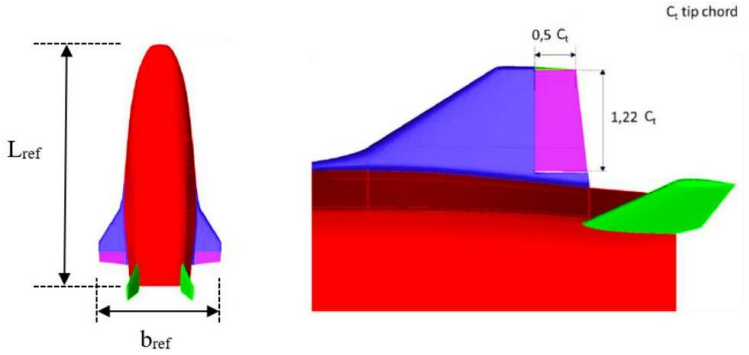

Figure 2 – Elevon and ruddervator sizing [4],[5].

The spatuled-body architecture allows to validate hypersonic aerothermodynamic design databases and passenger experiments, including thermal shield and hot structures, suitable for the successfully development of full-scale HSA [6],[7]. Within a typical mission scenario, in fact, HSA will encounter free-stream velocities ranging from hypersonic to low subsonic flow. This carefully demands attention while choosing the aircraft aeroshape which must be stable and maneuverable during both low and high-speed phases of flight [7]. The V-one aerodynamic assessment was undertaken with both numerical (i.e., CFD) and experimental (i.e., WT) approaches. Low Speed (LS) and HS (design point at M_∞=7) conditions were investigated. Subsonic LS aerodynamics rely on both CFD and WT investigations and results compared to validate numerical settings, while HS aerodynamics refers to CFD simulations only. CFD analyses are carried out at different attitudes and vehicle configurations (i.e., for different aerodynamic surfaces deflections). Then, an overview of the aerodynamic characteristics of the V-one aeroshape is performed with the goal to provide aerodynamic database (AEDB) to feed Flight Mechanics analyses.

Finally, it is worth noting that flowfield investigations are carried out with the commercial CFD code ANSYS FLUENT®, while the WT test campaign has been carried out at the University of Sydney.

2. Aerodynamic Analysis

Concept Aerodynamics is addressed for both low and high-speed flow conditions and results are provided in terms of force and moment coefficients, according to the ISO-1151 standard that is the convention usually adopted in Flight Mechanics. Lift (C_L), drag (C_D), side force (C_Y), rolling moment (C_l), pitching moment (C_m), and yawing moment (C_n) coefficients are calculated according to the following equations.

$$\begin{cases} C_i = \dfrac{2F_i}{\rho_\infty V_\infty^2 S_{ref}} & i = L, D, Y \\ C_j = \dfrac{2M_j}{\rho_\infty V_\infty^2 \eta_{ref} S_{ref}} & j = l, m, n \end{cases} \quad (1)$$

The moment coefficients refer to the moment reference centre (MRC), since vehicle's centre of gravity (CoG) position is not yet frozen. The reference length, η_{ref}, coincides to the fuselage length, L_{ref}, for the pitching moment calculations; while for roll and yaw the wing-span, b_{ref}, is assumed. Then, the vehicle planform area is considered as reference surface, S_{ref}. Lift, drag and pitching moment coefficients define the longitudinal characteristics of the aircraft; while the side force coefficient, rolling moment coefficient and the yawing moment coefficient determine the lateral-directional ones, see Figure 3. Positive directions of the force/moment coefficients as well as angles are shown in figure. Symmetric flap deflections (i.e., elevon mode) are positive when Trailing Edge (TE) is down. Positive asymmetric flap deflections (i.e., aileron model) are considered when the TE on the left wing is down. Ruddervator deflections are positive when the TE is deflected to the left.

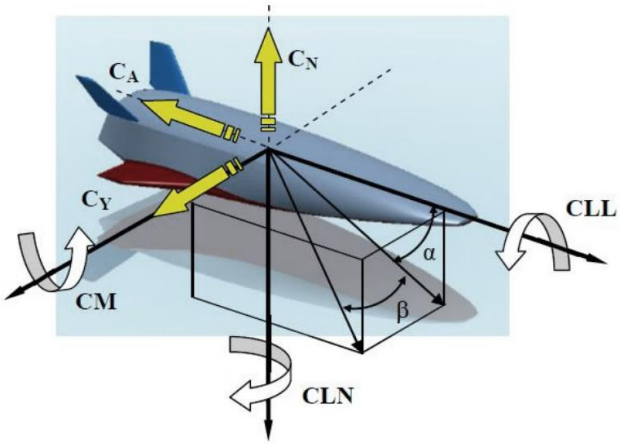

Figure 3 – Aerodynamic body reference frame with coefficients sign convention [4][5].

2.1 Low-speed Aerodynamics

Aircraft Aerodynamics at subsonic flow has been addressed by means of both WT and CFD investigations. This assessment is crucial for the design analysis about vehicle landing and complete recovery.

2.1.1 Wind tunnel subsonic analyses

The test campaigns analyzed aircraft aerodynamics at V_∞=30 m/s for a Re_∞=1.35x10^6. This condition was chosen as it could be easily replicated in the 7x5 foot LS facility at the University of Sydney. The model was fabricated using an assembly of 3D printed pieces, which were then glued together and sanded for a smooth finish. Components such as the wings and fins are removable to allow the testing of various control settings. The WT test model and measurements are summarized in Figure 4. Load cell measurements were taken in the body axis at 30 m/s through a range of angle of attack (AoA) and angle of sideslip (AoS) to determine aerodynamic and static stability derivatives for a clean configuration (i.e., no aerodynamic surfaces deflected). The load cell was enclosed within the body of the model to minimize the effect of the sting on the measurements.

Parameter	Description	Value	Units
L_{ref}	Vehicle body length	0.662	m
S_{ref}	Vehicle body wetted area	0.129	m^2
b_{ref}	Vehicle wingspan length	0.33	m

Figure 4 – Wind tunnel test model with dimensions [4], [5].

2.1.2 CFD subsonic analyses

The steady state, pressure based coupled solver was used for all CFD subsonic analyses. Flowfield simulations have been carried out at the same Reynolds number of the WT test to allow a fair comparison of data. The SST k-ω turbulence model was used for its ability to model separated flows and regions of circulation. Both unstructured and structured grids have been considered for the

computations. The unstructured mesh, shown in Figure 5, extends approximately 15 chord lengths upstream and 25 downstream and features tetrahedral cells in the field and prism inflation layers in the boundary layer, with Y^+=O(1) at wall. As shown, the mesh has a body of influence surrounding the vehicle for mesh refinement. For longitudinal simulations, a symmetry boundary condition is used to lower computation time, with the half body mesh comprising of about 7M cells. A full body mesh is considered for sideslip calculations with approximately double the number of elements.

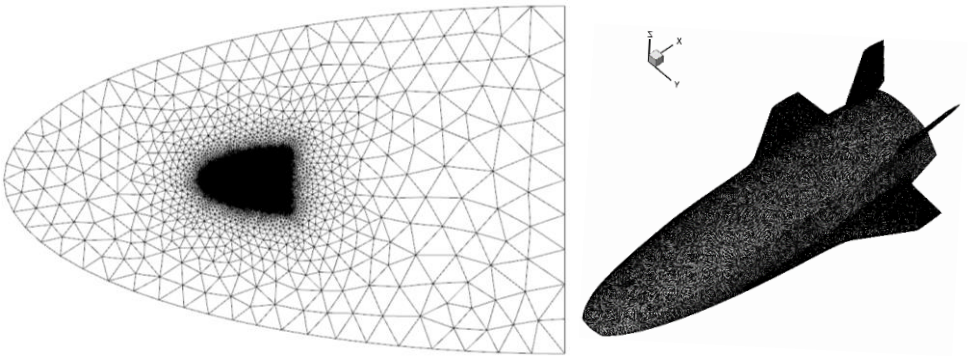

Figure 5 – Low Speed CFD Domain (unstructured grid) and vehicle surface Mesh [4][5].

The multiblock structured mesh, generated to address a sensitivity analysis about unstructured versus structured grid results, is shown in Figure 6. It has been generated by using ICEMCFD® software with 51 blocks for about 7M cells (half body).

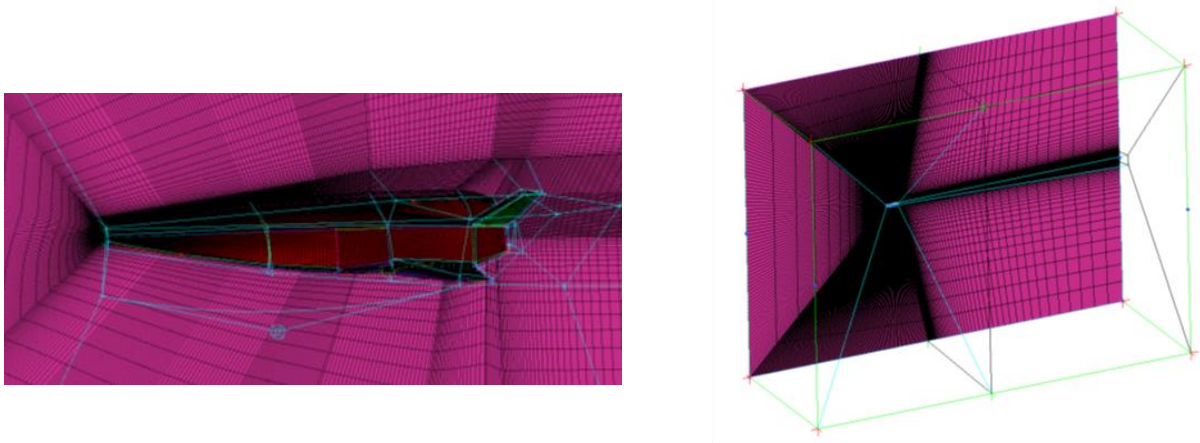

Figure 6 – Subsonic structured grid and aircraft surface Mesh [4][5].

2.2 CFD hypersonic analyses

The Reynolds Averaged Navier-Stokes (RANS) equations are integrated by means of the finite volume approach. The Flux Difference Splitting (FDS) second-order upwind scheme (least square cell based) has been used for the spatial reconstruction of convective terms, while for the diffusive fluxes a cell-centred scheme has been applied. An implicit scheme has been considered for time integration; while flow turbulence effects were simulated through the K-ω SST turbulence model applied to a steady state solution. The ideal gas model was assumed for air. Even though CFD simulations have been carried out at hypersonic flow conditions, the ideal gas assumption was still valid. The reason is that the aeroshape features a very slender configuration and shall fly at rather low AoA (i.e., weak attached shock waves). A temperature-dependent formulation was considered for the specific heat at constant pressure cp (i.e., thermally perfect gas) to accommodate the rather high flow energy [6].
As far as boundary conditions are concerned, the radiative cooled wall (ε=0.8) was assumed.
A multi-block structured grid was built for high-speed aerodynamic and aerothermodynamic investigations for clean configuration only, see Figure 7. The baseline grid topology for this work consists of 51 blocks for an overall number of about 7M cells (half body). Further, the mesh allows local refinement in order to improve numerical results, with the condition of Y^+=O(1) at wall.

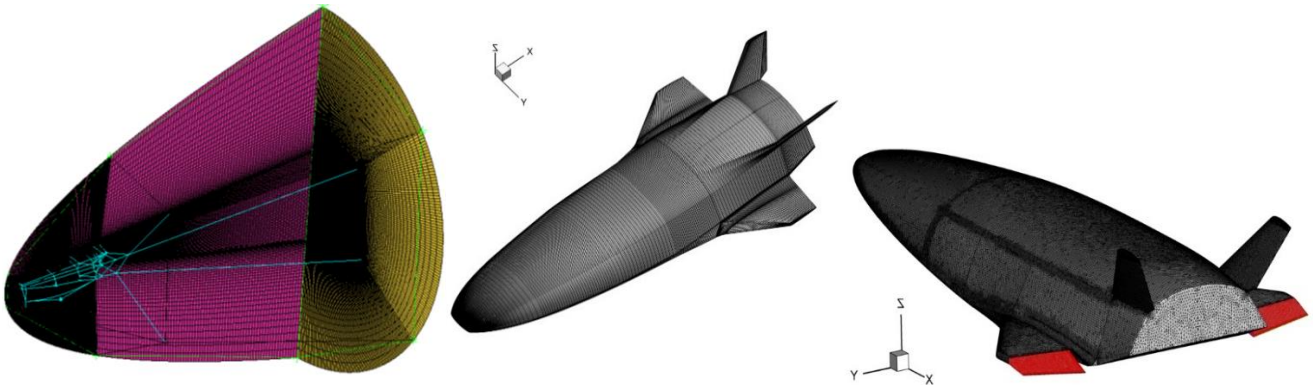

Figure 7 – High-speed mesh. Structured grid (left). Unstructured grid with deflected elevons (right) [4][5].

For elevon control authority studies, unstructured meshes are also generated as that provided in Figure 7 right side in the case of 10 degrees elevon deflection.

3. Aerodynamic Analysis

Aircraft low and high-speed Aerodynamics is summarized and discussed hereinafter.

3.1 Low-speed aerodynamic performances

A comparison between CFD and WT results for lift, drag, aerodynamic efficiency (L/D), and pitching moment coefficients is provided in Figure 8.

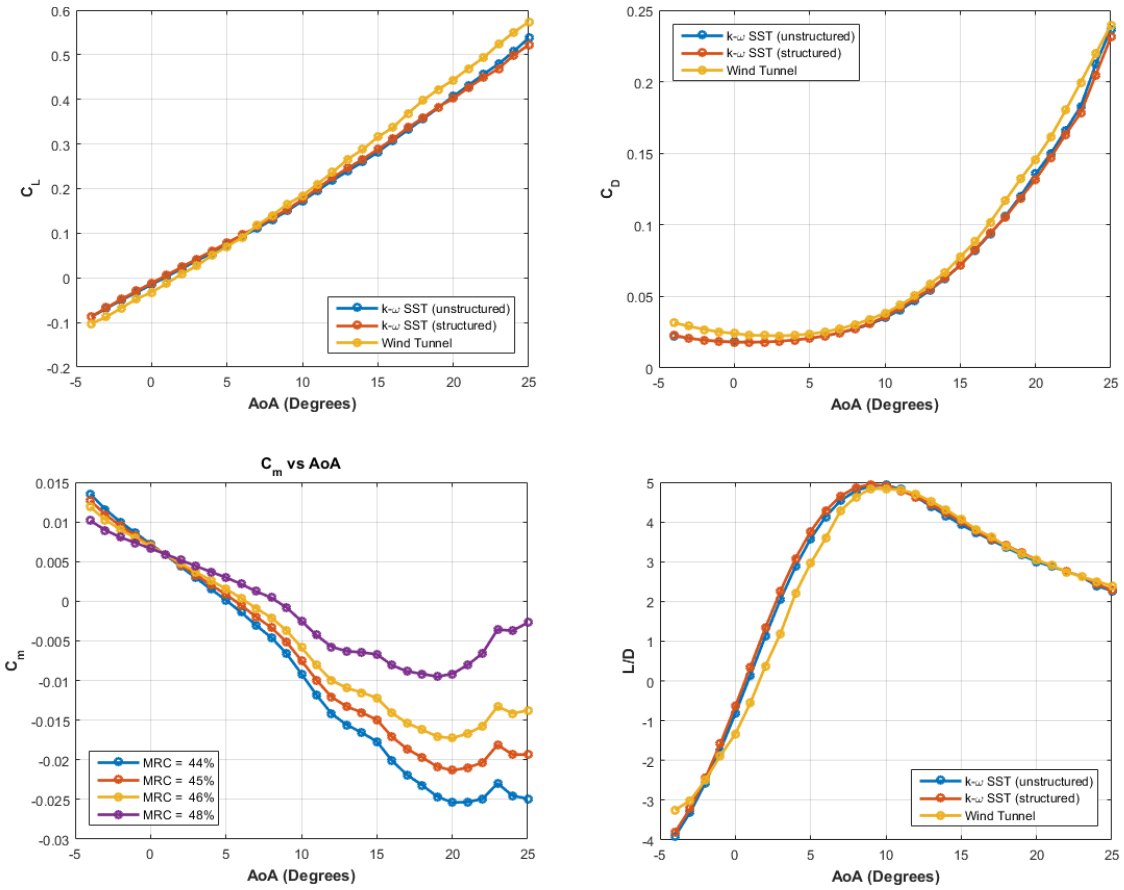

Figure 8 –WT and CFD results comparison for C_L, C_D, C_m (at different MRCs) and L/D coefficients versus α [4].

Lift coefficient features a non-linear lift curve slope, with a no clear stall condition from the CFD or the WT data. This behaviour is expected since the aircraft features a delta wing planform. The peak of

aerodynamic efficiency is approximately 5 and is found at about α=10°. Moreover, no difference between the structured mesh and the unstructured mesh was observed, so the unstructured mesh was used for the remainder of the simulations due to meshing simplicity, particularly for the control deflection cases. The development of vortices on the body of the vehicle with increasing AoA would explain the slight non-linearity in the lift curve slope and pitching moment results.
Further details can be found in Ref. [1].
As far as static longitudinal stability is concerned, a MRC location sensitivity analysis has been carried out by varying this reference point from 44 to 48% of L_{ref}. As shown, each of these MRC locations provide a negative gradient up to approximately α=20°, meaning all configurations are stable up to this point. On the base of these results a MRC at 45% of L_{ref} has been chosen for the prosecutions of aerodynamic investigations. Therefore, the vehicle landing speed needs to be high enough to avoid AoAs higher than 20 degrees.
Elevon deflection effects on aircraft aerodynamics is shown in Figure 9, where results from CFD studies carried out at d_e=-10°, -5°, 0°, 5°, and 10° are provided. As shown, positive deflections result in increased lift and drag and the separation between pitching moment curves suggests sufficient control authority for the aerodynamic control surfaces. In particular, trim angles of attack comprised from about -4° to 12° are possible while ranging elevon deflections from 10° to -10°.
Finally, no significant effect is expected on the maximum lift-to-drag ratio.

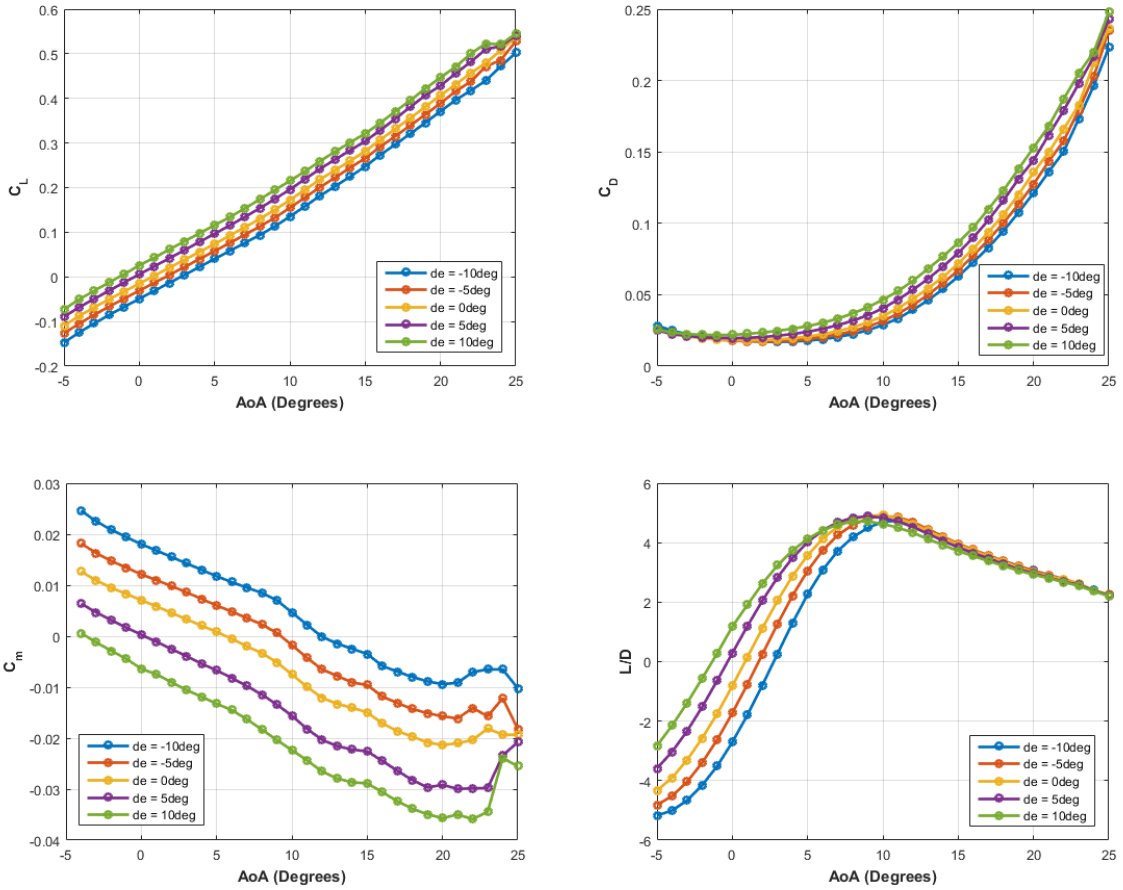

Figure 9 –CFD results for lift, drag, pitching moment and L/D coefficients vs AoA with varying elevon deflection angles and MRC at 45% L_{ref} [4].

Finally, sideslip effects on lateral-directional force (C_Y) and moment coefficients (C_l, C_n) for clean configuration are provided in Figure 10, where side slipslip, yaw and roll dervatives are aslo provided and compared to WT data. Results show negative slope of side force coefficient (i.e., stabilizing lateral force), thus demonstrating fin effectiveness. Positive derivatives through the entire range of AoA (i.e., $C_{n\beta}$>0) highight static stability in yaw; $C_{l\beta}$ derivative at low AoA is positive at low α but, fortunately, it changes sign becoming positive (stabilising in roll) at higher vehicle attitude.
Anyway, the roll instability at low α is not expected to impact aircraft controlability in the flight scenario foreseen for the flying-test bed.

Further, $C_{Y\beta}$, $C_{n\beta}$ and $C_{l\beta}$ derivatives are also provided and compared with tunnel data in Figure 10 right side. As shown, CFD and WT data trends compare well each other.

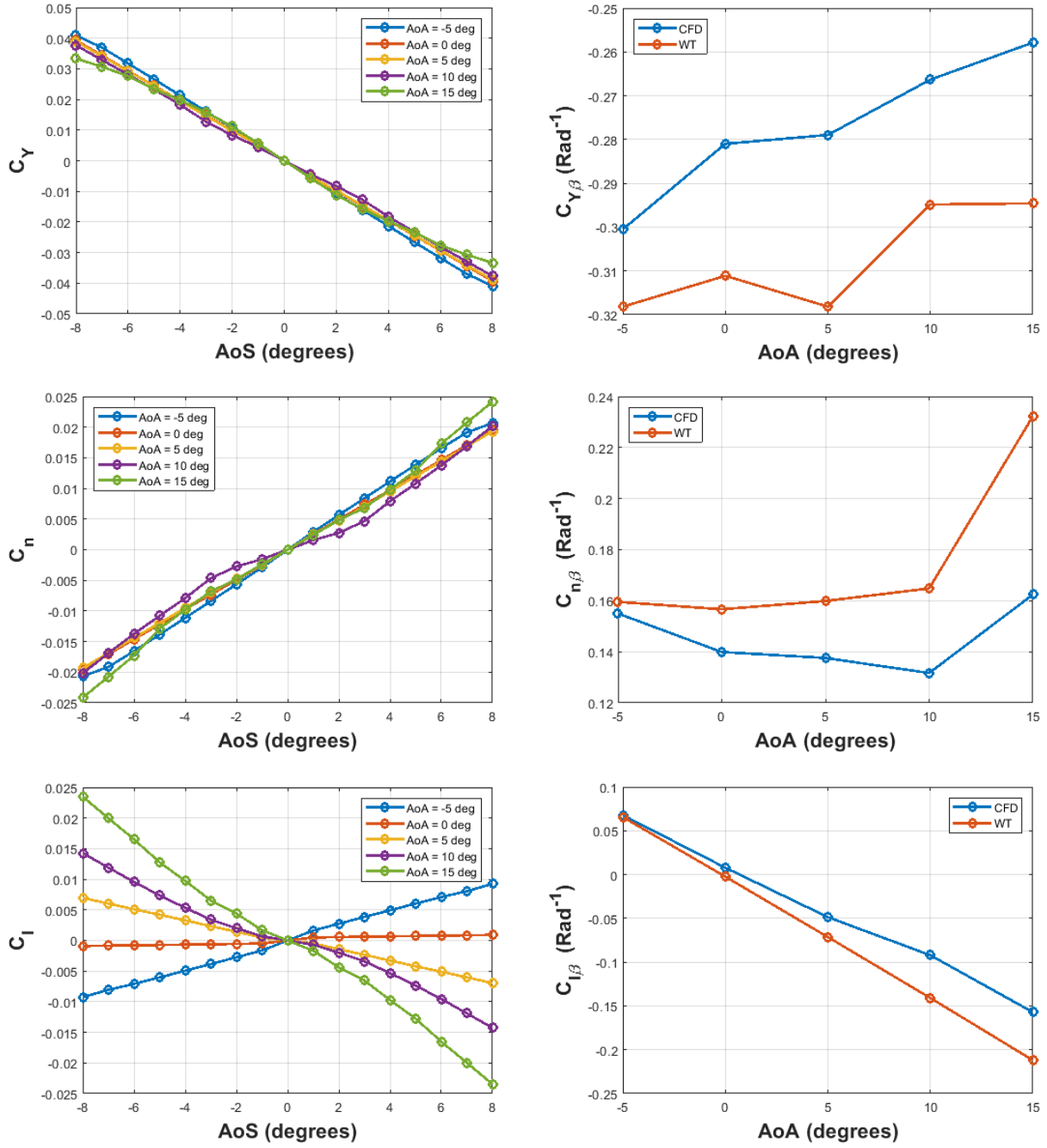

Figure 10 – Lateral-directional coefficients at MRC = 45% L_{ref} and WT/CFD comparison for derivatives vs AoA [5].

Further investigations on lateral-directional aerodynamic are provided for aileron and rudder deflections. For instance, Figure 11 provides elevon effectiveness throughout the AoA range, i.e. -5° to 15°.

Positive elevon deflection is seen to increase both the rolling and yawing moment coefficients. Increased effectiveness is seen with increasing AoA for roll, but for yaw while the derivative remains positive over the AoA range, elevon effectiveness in yaw control reduces for α>5°.

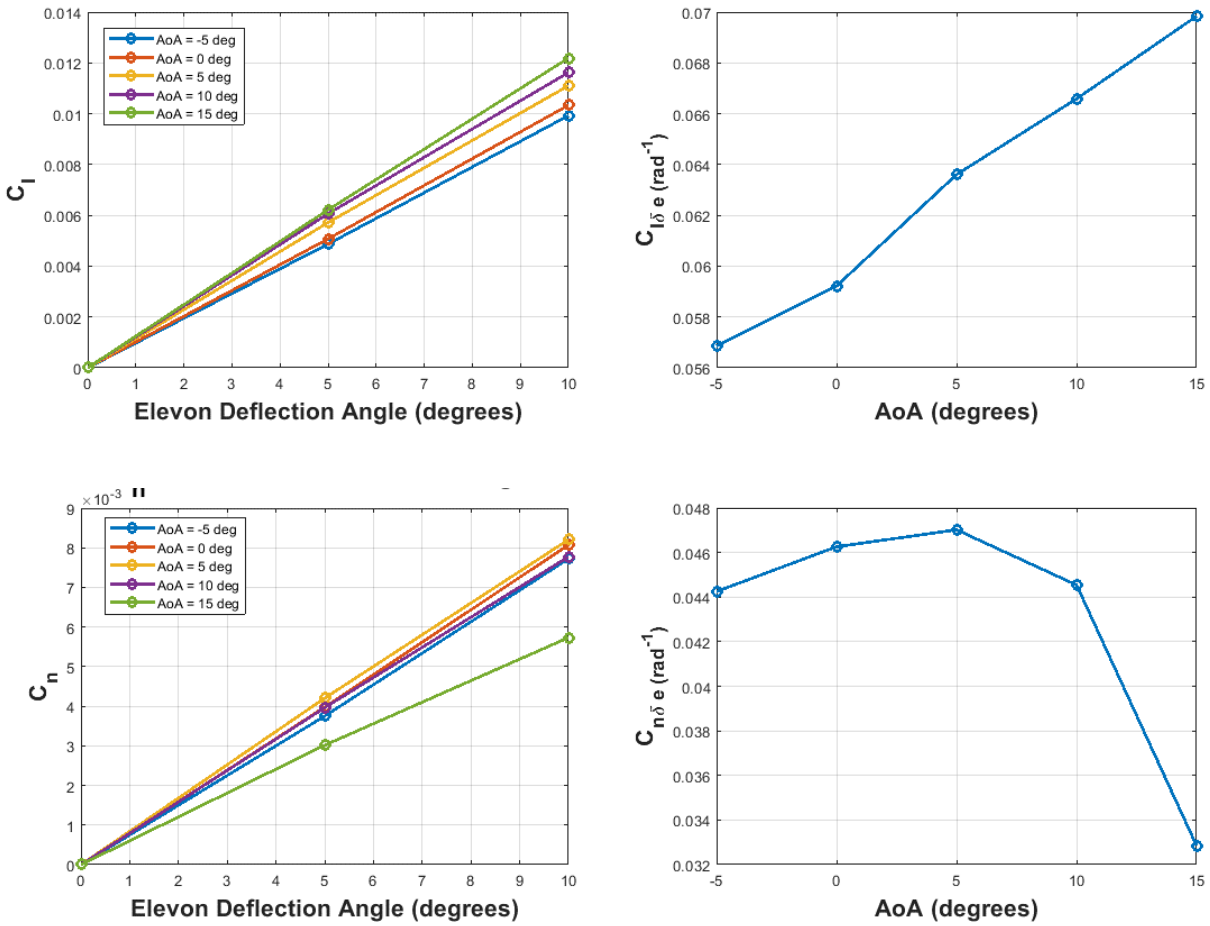

Figure 11 – Rolling and yawing moment coefficients vs elevon deflections and derivatives vs AoA [5].

Curves of side force coefficient vs rudder deflection angle as well as the control derivative show a maximum effectiveness at α=0° and a minimum at α=10°, thus highlighting that at high AoS and AoA, there is a sudden drop in force from the tailfins.
This is potentially due to stall or lower flow quality at the fins due to the forebody blocking the vertical tails from a clean flow path.
Same considerations can be inferred for the yawing as the side force from the fins is a major contributor to the C_n. Therefore, a reduced effectiveness in yaw from high rudder angle deflections is observed.
Results about rolling moment coefficients for various rudder deflections indicate that at low AoA, the rudders appear more effective than a high AoA, as expected.
This is also clearly confirmed by the decreasing values of $C_{l\delta r}$ derivative.

3.2 High-speed aerodynamic performances

High-speed Aerodynamics has been assessed for M_∞=7 and 30 Km altitude (Re_{Lref}= 12.5x10^6). This flight condition represents a design point of a scramjet-propelled aircraft in cruise condition.
Aerodynamic coefficients at this design point are provided in Figure 13, where lift, drag, L/D, and pitching moment coefficients are presented.

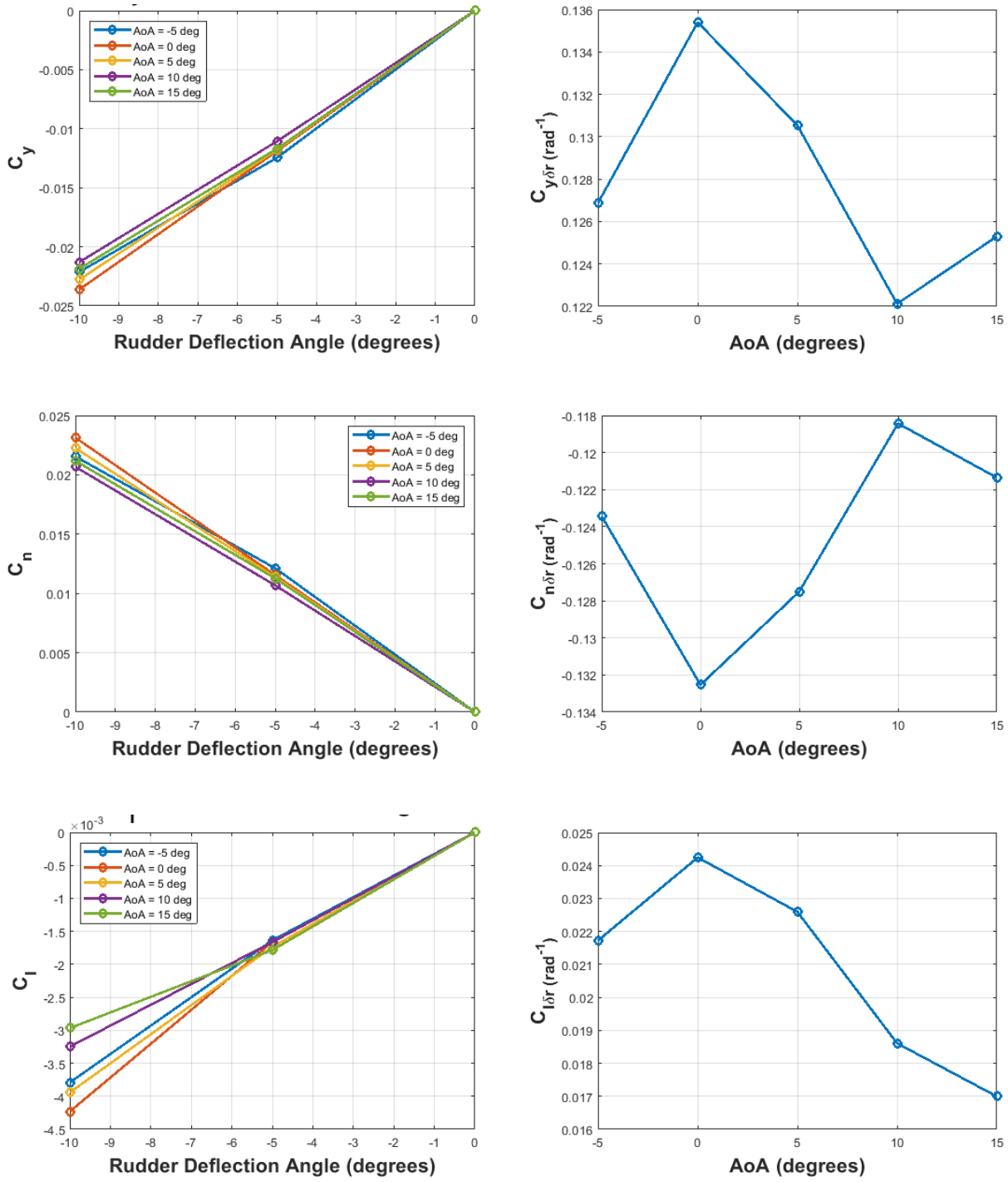

Figure 12 – Lateral-directional coefficients vs rudder deflections and derivatives vs AoA [5].

As one can see, the lift features a non-linear behaviour, as expected for the hypersonic flow conditions. The peak of L/D is attained at about α=10°. As in the low-speed conditions, a sensitivity analysis about the effect of MRC positions on C_m is carried out. Figure 13 shows that viable options of MRC positions are in the range (46÷44) % L_{ref}. In these cases, the aircraft features a natural trim point ranging from about α=7° to α=3°. The effect of sideslip flows on aircraft aerodynamics can be seen in Figure 14. This figure points out that the aircraft is statically stable in lateral-direction flight conditions for MRC at 45% L_{ref}. This is demonstrated by $C_{Y\beta}$<0, $C_{l\beta}$<0 (only at α=10 deg) and $C_{n\beta}$ always negative.

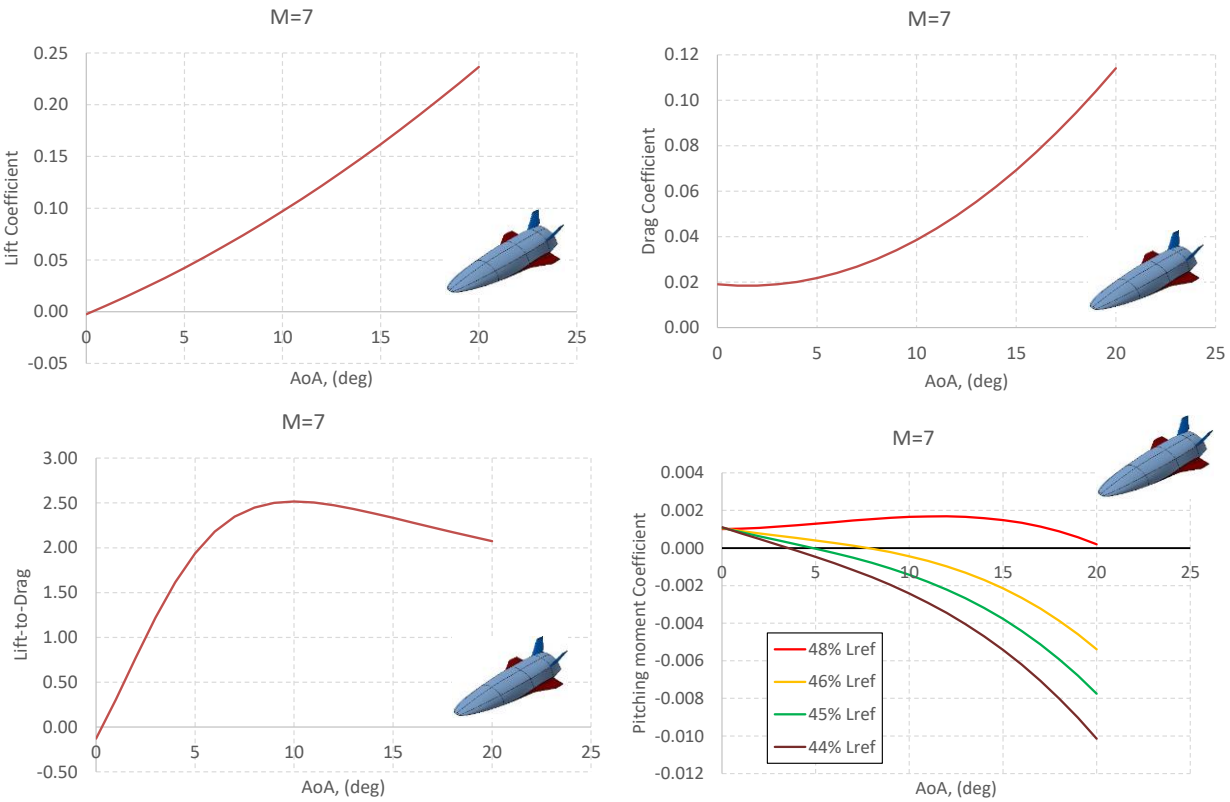

Figure 13 – Lift, drag, L/D and pitching moment coefficients vs AoA for clean configuration [4].

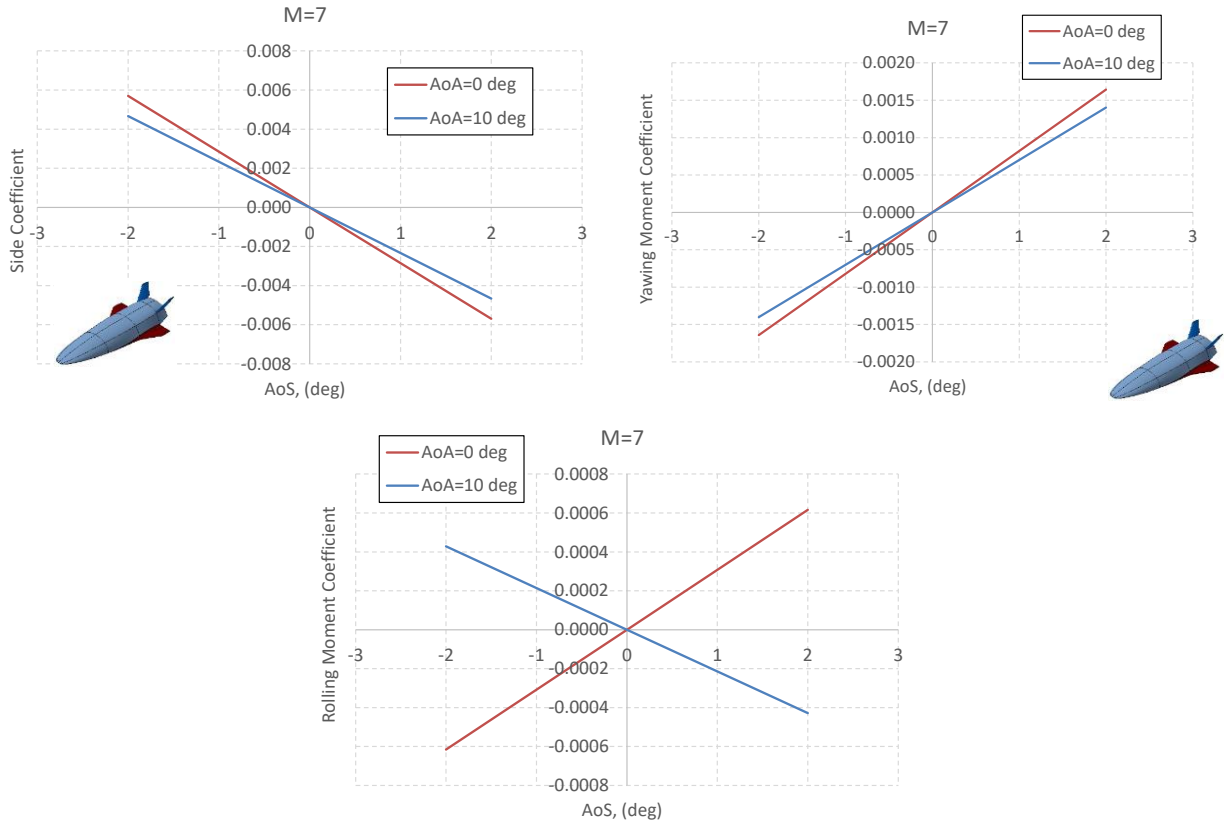

Figure 14 – Side, yaw, and rolling moment coefficients vs AoS for clean configuration [4].

The effect of d_e=±10° elevon deflections on the aircraft pitching moment is shown in Figure 15. As shown, control surface authority allows trimming the aeroshape in the range 1÷7 deg AoA.

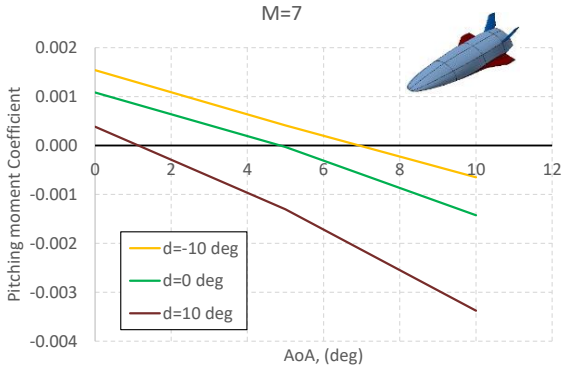

Figure 15 – Control surface authority aerodynamics for M_∞=7 and -10°≤d_e≤ 10°. MRC at 45% L_{ref} [4].

Aerodynamic control authority relies on wing flap deflections (i.e., both elevon and aileron). Therefore, the assessment of different aileron deflections is herein recognized. For instance, Figure 16 shows the effect of different aileron settings on all aerodynamic coefficients of the aircraft.

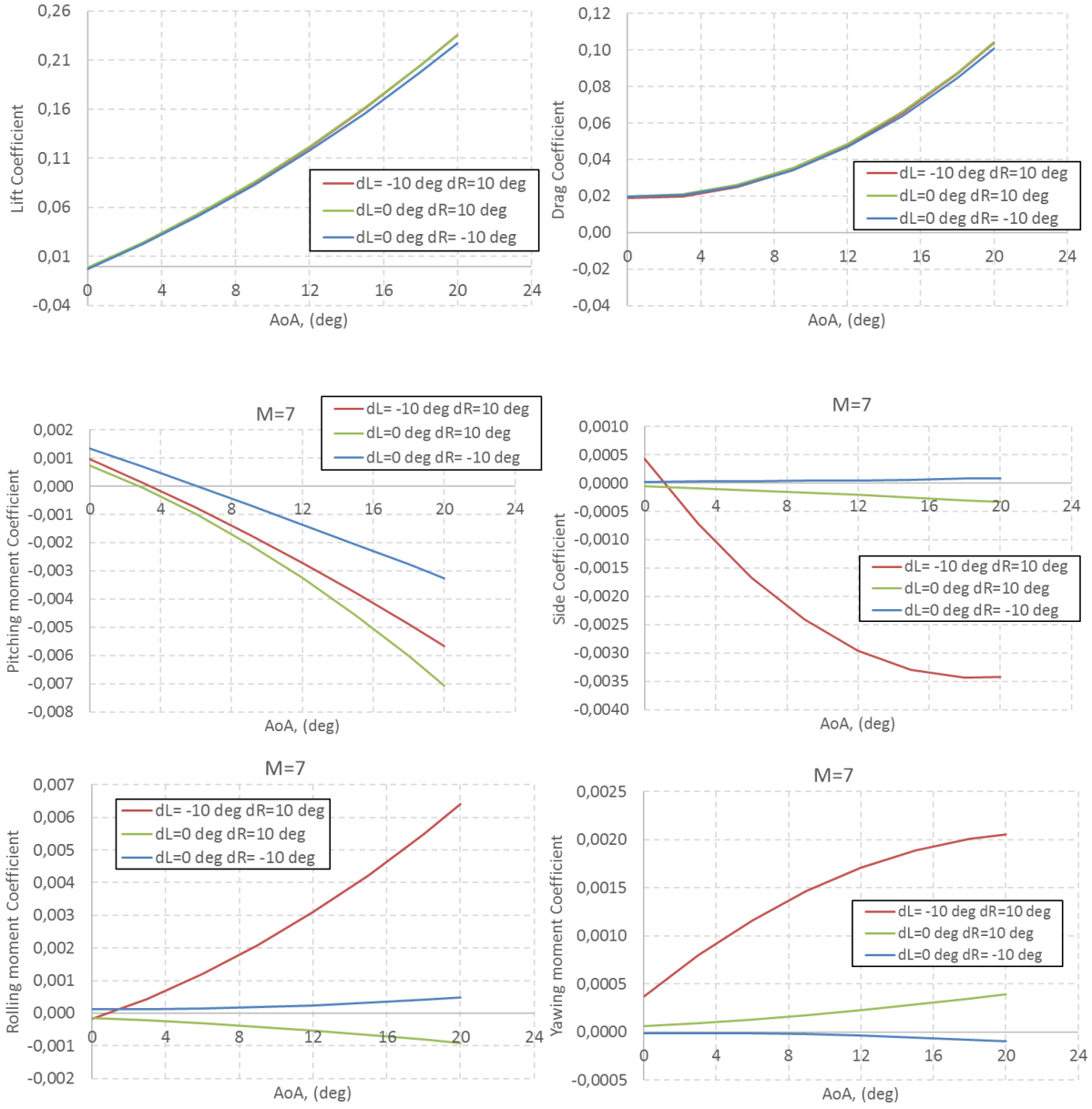

Figure 16 – Effects of different aileron setting on aircraft aerodynamics. MRC at 45% L_{ref} [5].

As shown, lift and drag are not affected by the investigated aileron setting; while the effect on the remaining force and moment coefficients appear remarkable.
As far as sideslip flow contribution on flapped configuration is concerned, Figure 17 shows aircraft aerodynamics for aileron deflection of 10 deg (i.e., d_L=-10° and d_R=10°) while AoS ranges from -8° to 8°.

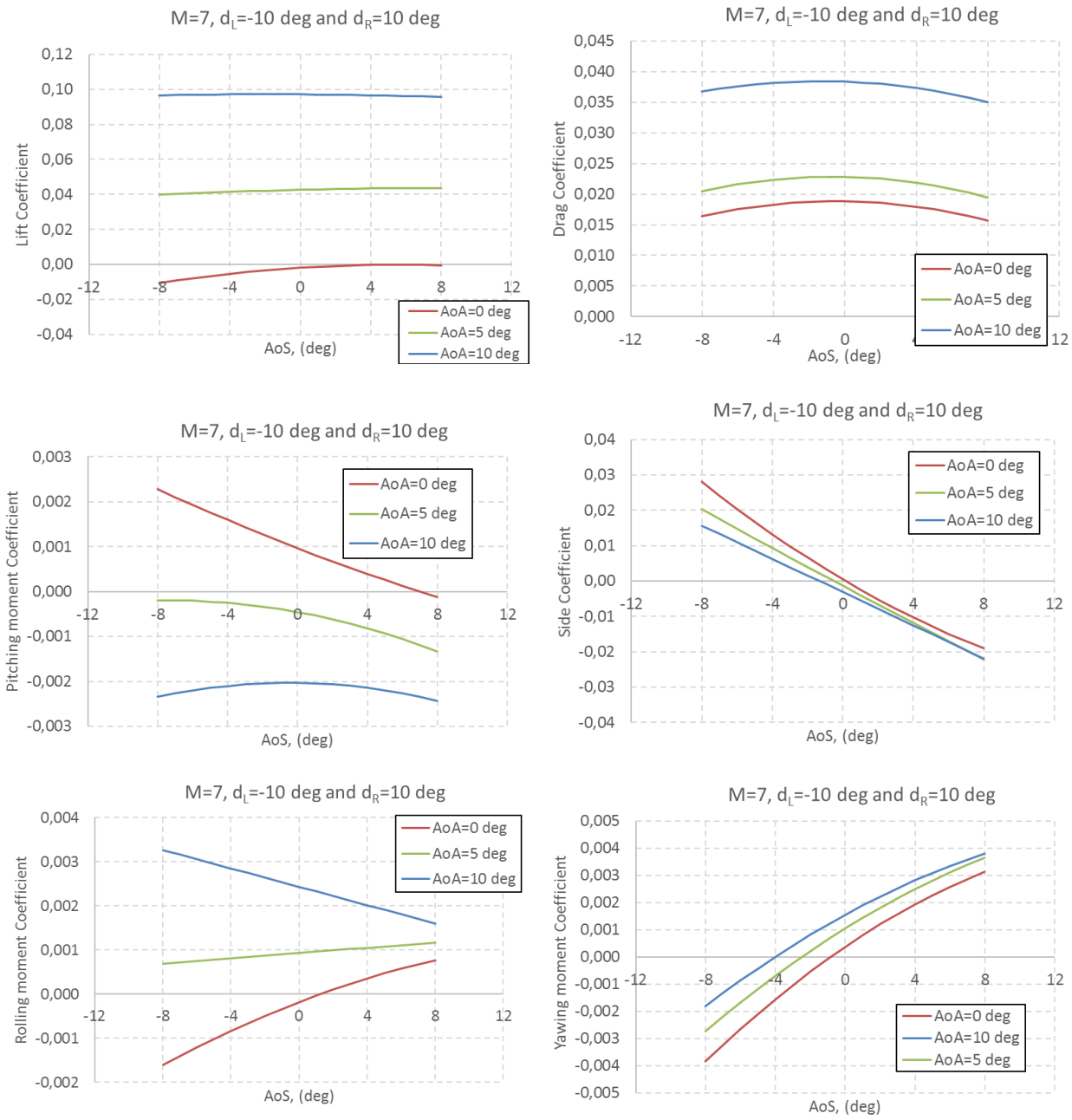

Figure 17 – Effects of AoS on 10 deg aileron deflections at α=0, 5 and 10 deg [5].

In this figure, concept aerodynamic force and moment coefficients are reported versus sideslip angle for three AoAs, namely 0, 5, and 10 deg. As shown, lift coefficients do not significantly change while the sideslip angle is ranging from -8 to 8 deg. However, for negative AoS and AoA=0 deg, the concept features negative lift, as expected. In fact, for this flow direction, only the aileron with negative deflection is working. The right aileron, even if with 10 deg deflection, is shadowed by the vehicle fuselage. On the other hand, C_D slightly decreases with AoS. Pitching moment coefficients versus β suggest that the aircraft features a longitudinal trim point at about β=7 deg when the concept is flying at α=0 deg.
Effects of sideslip angles on C_Y change in magnitude while α ranges from 0 to 10 deg, as expected.

Indeed, as soon as vehicle attitude increases, the aileron contribution to side force decreases due to wing and fuselage shielding effects.
Moreover, it is worth noting that sideslip derivative of side coefficient is negative, $C_{Y\beta}<0$. As known, this is one of the conditions needed to achieve lateral-directional static stability.
As far as C_l and C_n are concerned, Figure 17 highlights that when the concept is at α=0 deg roll moment nulls at about β=1 deg; while yawing moment equals zero at about -4 deg, -3 deg and -1 deg AoS for 10 deg, 5 deg, and 0 deg AoA, respectively. Further, it is worth to note that above results confirm that the vehicle is statically stable in lateral-directional flight for attitude larger than 5 deg AoA. Therefore, present aileron and vertical tails dimensions and positions seem to allow enough control authority of the vehicle concept for the given moment reference point.

4. Concluding Remarks

Flying test bed vehicles are an efficient way to experimentally validate next generation high-speed technologies. During a typical mission profiles, high-speed aircraft encounter different flow regimes ranging from hypersonic down to low subsonic and this requires a careful aeroshape design. The success of a mission demands an aerodynamically stable vehicle during both the high-speed and low-speed flight. In this framework, the paper focused attention on both experimental and numerical flowfield investigations carried out on a spatuled-forebody aeroshape. Wind tunnel data was compared with CFD simulations to assess the low-speed performance of the aeroshape. For high-speed flow conditions, only CFD analyses are available.
Initial findings for the hypersonic speed conditions point out that the high streamlined sharp leading edges of the V-one configuration led to a rather low wave drag component. Vehicle aerodynamics feature non-linear behaviour, as expected for the hypersonic speed flow conditions. The peak aerodynamic efficiency of about 2.5 is attained at approximately 10 degrees AoA. In particular, a statically stable configuration in both longitudinal and lateral-directional flight conditions demands a MRC position at 45% of fuselage length. Finally, the current sized elevon features a sufficient control authority.
Low speed aerodynamic analyses show that the lift coefficient features a mostly linear lift curve slope as expected for this flow regime and wing profile. The rounded leading edges of the double-delta planform prevent the formation of strong vortices, which would otherwise result in sharp changes in lift curve slope at high AoA. Vortices were instead observed forming along the forebody of the aircraft, which would contribute to aerodynamic forces and stability. Peak aerodynamic efficiency is found at about 10 degrees angle of attack, with a lift-to-drag ratio of approximately 5.
Static stability was achieved for most cases at the MRC suggested at the hypersonic analysis point but was not achieved at AoAs below 0 for rolling moment. While undesirable, it is expected that the vehicle will be at high AoA during the descent and landing phase and is not deemed a critical issue. A good correlation between numerical and experimental data exists, particularly for the longitudinal studies and that numerical simulations were a good indicator of stability when compared with the wind tunnel data. A comparison of a structured domain with an unstructured showed little difference in extracted coefficients.

5. Acknowledgement

The authors acknowledge the Sydney Informatics Hub and the use of the University of Sydney's high performance computing cluster, Artemis.

6. Contact Author Email Address

The contact author email address is giuseppe.pezzella@unicampania.it

7. Copyright Statement

References

[1] McClinton, C. R., Rausch, V. L., Nguyen, L. T., Sitz, J. R., “Preliminary X-43 flight test results”, Acta Astronautica, Volume 57, Issues 2–8, 2005, Pages 266-276, ISSN 0094-5765, https://doi.org/10.1016/j.actaastro.2005.03.060.

[2] Jeyaratnam, J., Bykerk, T., Verstraete, D., “Low speed stability analysis of a hypersonic vehicle design using CFD and wind tunnel testing” (2017) 21st AIAA International Space Planes and Hypersonics Technologies Conference, Hypersonics 2017, 10 p. DOI: 10.2514/6.2017-2223.

[3] Bykerk, T., Verstraete, D., Steelant, J., Low speed lateral-directional dynamic stability analysis of a hypersonic waverider using unsteady Reynolds averaged Navier Stokes forced oscillation simulations (2020) Aerospace Science and Technology, 106, art. no. 106228. DOI: 10.1016/j.ast.2020.106228

[4] Bykerk, T., Verstraete, D., Pezzella, G., Viviani, A. “High and Low Speed Analysis of a Re-usable Unmanned Re-entry Vehicle”. HISST. International Conference on High-Speed Vehicle Science and Technology. Moscow. Russia. November 25-29, 2018. hisst-2018_1620897.

[5] Bykerk, T., Pezzella, G., Verstraete, D., Viviani, A. “Lateral-Directional Aerodynamics of a Re-Usable Re-Entry Vehicle”. 8th European Conference for Aeronautics and Space Sciences (Eucass-2019). July 2019. Madrid. Spain.

[6] Scigliano, R., Pezzella, G., Di Benedetto, S., Marini, M., Steelant, J., “Hexafly-Int Experimental Flight Test Vehicle (EFTV) Aero-Thermal Design”. Proceedings of the ASME 2017 International Mechanical Engineering Congress & Exposition IMECE 2017. November 3-9, 2017, Tampa, Florida, USA. ASME 2017 International Mechanical Engineering Congress and Exposition Volume 1: Advances in Aerospace Technology Tampa, Florida, USA, November 3–9, 2017.Conference Sponsors: ASME. ISBN: 978-0-7918-5834-9. Paper No. IMECE2017-70392, pp. V001T03A022; 14 pages doi:10.1115/IMECE2017-70392

[7] Schettino, A., Pezzella, G., Marini, M., Di Benedetto, S., Villace, V.F., Steelant, J., Choudhury, R., Gubanov, A., Voevodenko, N. “Aerodynamic database of the HEXAFLY-INT hypersonic glider”. (2020) CEAS Space Journal, 12 (2), pp. 295-311. DOI: 10.1007/s12567-020-00299-4